ORIGINAL ARTICLE

Differentiation of Primary Cardiac Tumors from Metastatic Tumors by Non-invasive Cardiac Imaging

Yoichi Otomi, MD, PhD[1)], Hideki Otsuka, MD, PhD[2)], Maki Arase, MD[1)], Hiroki Arase, MD[3)], Hirotsugu Kurobe, MD, PhD[3)], Tetsuya Kitagawa, MD, PhD[3)] and Masafumi Harada, MD, PhD[1)]

Received: November 17, 2017/Revised manuscript received: February 13, 2018/Accepted: March 9, 2018
J-STAGE Advance published: July 17, 2018

Abstract

***Background*: Various imaging modalities are used to identify and characterize cardiac masses. While echocardiography remains the preferred imaging modality to evaluate cardiac masses, computed tomography (CT), magnetic resonance imaging (MRI), and ^{18}F-fluorodeoxyglucose positron emission tomography (^{18}F-FDG PET)/CT are being increasingly employed to assess cardiac mass lesions. However, the clinical value of non-invasive cardiac imaging for differentiating between primary cardiac mass and metastatic lesions has not yet been examined in detail. The purpose of the present study was to evaluate the diagnostic utility of non-invasive cardiac imaging for differentiating primary cardiac tumors from metastatic lesions, and non-tumorous lesions.**

***Methods*: A retrospective review was conducted on 22 cardiac mass lesions in 20 patients assessed by cardiac imaging (at least one of CT, MRI, or ^{18}F-FDG PET/CT) between December 2005 and March 2017. CT findings included the tumor size, location, existence of calcification, and morphology of the base portion of the lesion. MRI parameters included signals with T1-weighted imaging (T1WI), T2WI, mobility with cine imaging, and contrast enhancement. Tracer uptake by each cardiac lesion using ^{18}F-FDG PET/CT was also evaluated.**

***Results*: Among 17 cardiac mass lesions assessed by contrast-enhanced CT, all cardiac myxomas and papillary fibroelastomas had a pedunculated base portion. All metastases located in the cavity had a sessile base portion (P=0.0035). Malignant tumors (metastases and malignant lymphoma) had no mobility, while cardiac myxomas had a slightly higher frequency of mobility with cine MRI (0% vs. 100%, P=0.0667). Among the four lesions for which ^{18}F-FDG PET/CT was performed, the three malignant lesions had strong ^{18}F-FDG uptake, while the benign lesion showed insignificant accumulation.**

***Conclusions*: The characteristics of the base portion of cardiac mass were useful for differentiating primary cardiac tumors from metastatic cardiac tumors. Cine MRI also exhibited diagnostic utility for differentiating between primary cardiac tumors and metastases. Therefore, non-invasive cardiac imaging may be employed to differentiate cardiac mass lesions. The accurate diagnosis of cardiac mass lesions may require the assessment of multiple characteristics on images.**

Keywords: Cardiac mass lesion, Cardiac myxoma, Cardiac tumor, Papillary fibroelastoma, Tomography
Ann Nucl Cardiol 2018; 4 (1): 23−33

doi: 10.17996/anc.18-00050

1) Yoichi Otomi, Maki Arase, Masafumi Harada
Department of Radiology, Tokushima University Hospital, Tokushima, 2-50-1 Kuramoto-cho, Tokushima 770-8503, Japan
E-mail: otomi.yoichi@tokushima-u.ac.jp
2) Hideki Otsuka
Department of Medical Imaging/Nuclear Medicine, Institute of Biomedical Sciences, Tokushima University Graduate School, Tokushima, Japan
3) Hiroki Arase, Hirotsugu Kurobe, Tetsuya Kitagawa
Department of Cardiovascular Surgery, Institute of Biomedical Sciences, Tokushima University Graduate School, Tokushima, Japan

Cardiac mass lesions are classified as neoplastic or non-neoplastic lesions. Neoplastic lesions are further divided into primary benign, primary malignant, and metastatic lesions (1). The autopsy incidence of primary cardiac malignant lesions is 0.0017 to 0.33% (1-4). Among primary cardiac tumors, 75% of primary cardiac lesions are benign and remaining 25% are malignant (5). The most common primary benign cardiac mass are cardiac myxomas, which account for 50% of all primary cardiac lesions (5). Metastatic cardiac lesions are more common than primary malignant lesions in adult populations (6) and are found in 10-12% of cancer patients based on autopsy results (7-9).

Non-neoplastic lesions, such as thrombi, are also found in the cardiac cavity. In recent years, the early diagnosis of cardiac masses has been possible using advanced diagnostic technology such as echocardiography, computed tomography (CT), magnetic resonance imaging (MRI), and ^{18}F-fluorodeoxyglucose positron emission tomography (^{18}F-FDG PET). Table 1 summarized the typical characteristics of cardiac masses in each modality. Different treatment strategies are employed for primary cardiac mass and metastatic lesions. Differentiating between these two conditions may contribute the treatment strategy of these patients. Therapy for benign primary cardiac tumors is surgical resection, which provides excellent long-term survival for most patients, particularly those undergoing complete resection (10, 11). In contrast, systemic chemotherapy applies in patients with cardiac metastases. Some patients have surgical resection, or palliative care (12-15). Although it is important to distinguish between primary cardiac and metastatic cardiac masses, currently there are limited diagnostic approaches (16, 17). Life threating complications, include arrhythmia and embolism, in patients having cardiac mass be fatal. Therefore, an accurate diagnosis and treatment strategy are important. In this regard the purpose of the present study was to evaluate the diagnostic utility of non-invasive cardiac imaging for differentiating primary cardiac tumors, from metastatic lesions, or non-tumorous lesions.

Materials and methods

Study population

A retrospective review was conducted on 22 cardiac mass lesions in 20 patients (11 females and 9 males, mean age; 62.4 years old) assessed by non-invasive imaging (at least one of CT, MRI, or ^{18}F-FDG PET/CT) between December 2005 and March 2017 at Tokushima University Hospital. These patients underwent cardiac imaging for the evaluation of cardiac masses, and a total of 22 cardiac mass lesions were examined for this study.

The definition of a cardiac mass included intracavity, valvular, and pericardial masses initially identified by non-invasive imaging modality studies including echography, CT, or ^{18}F-FDG PET/CT.

This study was approved without the need for individual informed consent by our Institutional Ethics Committee and was conducted in accordance with the 1964 Declaration of Helsinki and its later amendments.

Diagnostic imaging parameters

The size, location, existence of calcification, and morphology of the base portion (pedunculated, sessile, or multi-legged) of cardiac lesions by CT were summarized. Signals by T1-weighted imaging (T1WI) and T2WI, mobility by cine imaging, and contrast enhancement by MRI were also summarized. Uptake by each cardiac lesion using ^{18}F-FDG PET/CT was also evaluated.

Data acquisition

Cardiac CT

The patients underwent a CT scan using a 16-slice MDCT scanner (Aquilion 16; Toshiba Medical Systems, Otawara, Japan) or 320-slice MDCT scanner (Aquilion ONE; Toshiba Medical System, Otawara, Japan). CT scanning parameters were as follows: 120 kV with the tube current automatically set by the exposure control system and a 0.5-second tube rotation time. Iodinated contrast material was intravenously injected using an automatic power injector. CT was performed without ECG synchronism, except for one lesion (13, 18).

Cardiac MRI

Cardiac MRI was performed using a 1.5-Tesla MRI scanner (SIGNA EXICE 1.5T; GE Medical Systems, Milwaukee, WI, USA) with electrocardiography triggering and an 8-channel cardiac coil. MRI scan included T1 black-blood fast spin echo images in the short axis, and T2 black-blood with fat-suppressed fast spin echo images in the short and long axes. Cine MR sequences (FIESTA) in the short axis, in the long axis, and in the four-chamber view were also obtained. After the injection of gadolinium-based contrast agent, we obtained post-contrast T1 black-blood fast spin echo images through the center of the cardiac mass (12, 19).

^{18}F-FDG PET/CT

^{18}F-FDG was synthesized with the nucleophilic substitution method using an FDG-synthesizing instrument (F100, Sumitomo Heavy Industries, Ltd., Tokyo, Japan) and a cyclotron (CYPRIS, Sumitomo Heavy Industries, Ltd., Tokyo, Japan) at our institution. Patients fasted for at least 6 hours and blood glucose levels were evaluated prior to FDG administration. In the case of a blood glucose level <140 mg/dl, patients received an intravenous administration of 3.7 MBq/kg of ^{18}F-FDG (20). Patients were instructed to remain resting on a bed to minimize muscle FDG uptake before the scan. ^{18}F-FDG

Table 1 Image findings of representative cardiac tumors (modified from Ref. 1, 5-9)

	Modality	CT	MRI	FDG PET/CT
Neoplastic lesion	Location			
Benign				
Myxoma	LA>RA	Pedunculated, low density	Generally mobile on cine images, CE moderate (+)	Weak to mild FDG uptake
Papillary fibroelastoma	Valves	Small, pedunculated	Generally mobile on cine images	Weak FDG uptake
Fibroma	LV>RV	Low density, central calc.	T2WI-low, CE minimal	Mild FDG uptake, rarely strong
Lipoma	Varies	Homogeneous low density (CT value: less than -50 HU)	T1WI-hyper, CE minimal	No FDG uptake
Rhabdomyoma	LV>RV	Density similar to the myocardium	T1WI-iso to marginally hyper, T2WI-hyper, CE moderate	-
Malignant				
Angiosarcoma	RA>RV, pericardium	Broad base, inhomogeneous, low density, infiltrative	T2WI-inhomogeneous, inhomogeneous CE (+)	Strong FDG uptake
Osteosarcoma	LA>RA, RV	Broad base, low density, infiltrative, extensive calcification	T1WI-iso, T2WI-hyper	-
Lymphoma	RA	Infiltrative, inhomogeneous CE (+)	T1WI-iso, CE variable	Commonly strong FDG uptake
Metastasis	Varies	Inhomogeneous CE (+)	Typically T1WI-low, T2WI-hyper (non-specific)	Strong FDG uptake
Non-neoplastic lesion				
Thrombus	RA>LV, LA	Low density	T2WI-low, CE (-), peripheral CE in chronic lesions	Weak FDG uptake

LA: left atrium, LV: left ventricle, RA: right atrium, RV: right ventricle, iso: iso-intensity, hyper: hyper-intensity, CE: contrast enhancement, HU: Hounsfield units

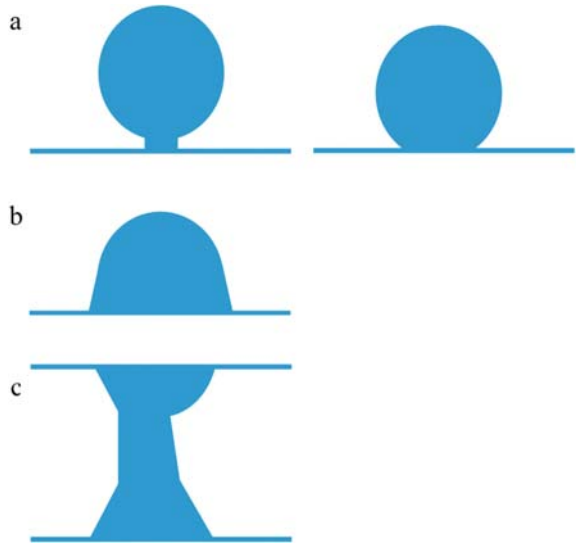

Fig. 1 The morphology of the base portion by contrast-enhanced CT. (**a**) Pedunculated (right: semi-pedunculated, left: pedunculated), (**b**) sessile, and (**c**) multi-legged.

PET/CT image acquisition started 1 hour after the ^{18}F-FDG injection with the patient in a relaxed supine position using an integrated PET/CT scanner (Aquiduo, Toshiba Medical Systems Corporation, Otawara, Japan). A total-body low-dose CT scan underwent for the calculation of attenuation correction. CT images were obtained using a standardized protocol involving 120 kV and a tube-rotation time of 0.5 second per rotation. PET images consisted of eight bed positions with a 2-min per table position over the same region using the three-dimensional high-sensitivity mode. PET images reconstruction included a 128×128 matrix with 1.34 zoom using an ordered-subset expectation maximization (OSEM) iterative reconstruction algorithm employing 14 subsets and 4 iterations, and the CT-based attenuation correction. Noise was reduced by smoothing the resultant images with a Gaussian filter of 8.0 mm full width at half maximum.

Image interpretation

Cardiac CT

In cardiac CT, we evaluated the following parameters on the viewer (Centricity universal viewer, GE Healthcare, Wisconsin, USA): 1. location of the cardiac mass, 2: cardiac mass size, 3: the presence or absence of calcification or fat, and 4: the morphology of the base portion (pedunculated, sessile, or multi-legged) (21-23). Calcified lesions in the cardiac mass were estimated by the maximum CT number. Representative images of each morphology of the base portion are shown in Fig. 1.

Cardiac MRI

In MRI, we evaluated the following parameters on the viewer (Centricity universal viewer, GE Healthcare, Wisconsin, USA): 1: intensity on T1WI, 2: intensity on T2WI, 3: existence or absence of contrast enhancement after the gadolinium injection, and 4: mobility by cine imaging (19, 24-26). Representative images of mobility or non-mobility by cine imaging are shown in Fig. 2.

^{18}F-FDG PET/CT

Positive myocardial uptakes in the left ventricle were evaluated visually. The maximum standardized uptake value

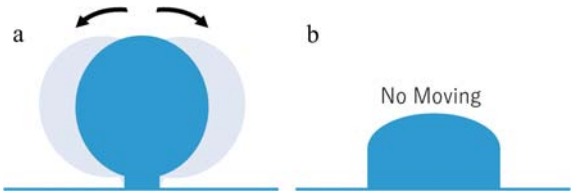

Fig. 2 Mobility based on cine MRI. (**a**) Mobile (+) and (**b**) non-mobile (-).

(SUV_{max}) was measured by drawing a region of interest (ROI) on each cardiac mass lesion through all PET images on the viewer (AW server 2.0, GE Healthcare, Wisconsin, USA) referencing CT images. However, we did not include LV physiological myocardial uptake or physiological uptake on the liver parenchyma (27, 28). Findings obtained by whole-body PET/CT were also evaluated.

Statistical analysis

Parameters were expressed in terms of the mean ± standard deviation (SD). Patient characteristics were compared by an unpaired *t*-test between patients with malignant lesions and those with benign lesions. Fisher's exact probability test was used to assess differences in the morphology of the base portion between primary cardiac tumors (papillary fibroelastomas and cardiac myxomas) and metastases. Fisher's exact probability test was also used to assess differences in mobility by cine MRI between cardiac myxomas and malignant lesions (metastases and malignant lymphomas). A statistical software program (SPSS Statistics version 24, IBM, Chicago, IL, USA) was used for analyses. A p value less than 0.05 was considered to be significant.

Results

Patient background

Table 2 shows patient characteristics including the age, gender, height, body weight, left ventricular ejection fraction (LVEF), New York Heart Association (NYHA) functional class, and electrocardiogram (ECG) findings of 6 patients with malignant cardiac mass lesions and 14 patients with benign cardiac mass lesions. None of the patients examined had benign and malignant lesions. There were no significant differences in age (p=0.788), gender (p=0.085), height (p=0.670), weight (p=0.419), or LVEF (p=0.502) between the two groups.

Types of cardiac mass lesions (malignant and benign lesions)

Table 3 shows the diagnosis and imaging findings of cardiac mass lesions. The diagnoses of cardiac masses were as follows: 5 cardiac myxomas (Fig. 3), 5 papillary fibroelastomas (Fig. 4), 5 metastases (Fig. 5), 3 thrombi (Fig. 6), 1 malignant lymphoma (Fig. 7), 1 rhabdomyoma, 1 lipoma, and 1 vegetation. Fifteen lesions (5 cardiac myxomas, 5 papillary fibroelastomas, 2 thrombi, 1 rhabdomyoma, 1 lipoma, and 1 vegetation) were histologically confirmed by surgery. The other 7 lesions (5 metastases, 1 malignant lymphoma, and 1 thrombus) were clinically diagnosed. Six lesions (5 metastases and 1 malignant lymphoma) were categorized as malignant lesions, while the other 16 (5 cardiac myxomas, 5 papillary fibroelastomas, 3 thrombi, 1 rhabdomyoma, 1 lipoma, and 1 vegetation) were defined as benign. The details of the 6 malignant lesions were as follows: 1. metastasis of squamous cell carcinoma of the lung, 2. metastasis of esophageal squamous cell carcinoma, 3. metastasis of breast cancer (adenocarcinoma), 4. metastasis of uterine leiomyosarcoma, 5. metastasis of lung leiomyosarcoma, and 6. Non-Hodgkin's lymphoma, cutaneous T-cell lymphoma.

Cardiac imaging data

Contrast-enhanced CT (CECT) was performed on 18 lesions. Plain CT alone was employed for 3 lesions, and the low-dose CT of ^{18}F-FDG PET/CT without a conventional CT examination was performed on 1 lesion. MRI was conducted on 6 lesions. ^{18}F-FDG PET/CT was performed on 4 lesions.

CT Findings

Two lesions showed calcification on the cardiac mass (1 cardiac myxoma and 1 thrombus). The maximum CT number of cardiac myxoma was 1111 Hounsfield units (HU), and that of the thrombus was 154 HU.

Excluding 2 lesions (an intramyocardial lesion and a lesion in the wall of the interventricular septum), we evaluated the morphology of the base portion in 16 out of 18 lesions on which CECT was performed. Ten lesions (5 cardiac myxomas and 5 papillary fibroelastomas) had a pedunculated base portion. Four lesions (3 metastases and 1 vegetation) had a sessile base portion. Two lesions (2 thrombi) had a multi-legged base portion. Primary cardiac tumors (cardiac myxomas and papillary fibroelastomas) had a pedunculated base portion, and metastases located in the cavity had a sessile base portion (10/10 (100%) vs. 0/3 (0%) p=0.0035) (Fig. 8).

Four out of the five cardiac myxomas (80%) were attached to the interatrial septum of the left atrium, while the remaining lesion was attached to the lateral wall of the LV. Four out of the five papillary fibroelastomas (80%) were attached to the aortic valve, while the other was attached to the lateral wall of the left atrium. Three out of the five metastases were located in the cardiac cavity, and these lesions were attached to the right ventricle, LV, and left atrium (one each). One metastasis was located in the wall of the interventricular septum, while another was located along the left aspect of the pericardium.

Table 2 Patient characteristics (n=20)

	Malignant (n=6)	Benign (n=14)	p value
Age (years old)	60 ± 12	63 ± 25	0.788
Gender (male)	1 (17%)	8 (57%)	0.085
Height (cm)	151 ± 14	146 ± 29	0.670
Weight (kg)	4 ± 7	51 ± 16	0.419
LVEF (%)	63 ± 8	65 ± 4	0.502
NYHA functional class (median)	1	1	
ECG abnormalities			
Accelerated idioventricular rhythm	1		
Sinus tachycardia	1		
Atrial fibrillation		3	
ST-T abnormalities		3	
Abnormal Q wave		2	
Ventricular tachycardia		1	
Complete right bundle branch block		1	

Data are represented as the mean ± SD. NYHA: New York Heart Association, LVEF: left ventricular ejection fraction, ECG: electrocardiogram.

Table 3 Summary of the diagnosis and imaging findings of cardiac mass lesions

No.	Age (y)	Gender	Diagnosis	Location	Size (mm)	Radiologic findings
Malignant lesions						
1	67	F	Meta. Lung (Sq)	RV	41 × 32	CT (sessile, calc. -), MRI (iso-intensity on T1WI, hyper-intensity on T2WI, no mobility, CE+)
2	62	F	Meta. Esophagus (Sq)	LV	32 × 26	CT (sessile, calc. -), MRI (iso-intensity on T1WI, inhomogeneous predominantly high intensity on fat-suppressed T2WI, no mobility, CE+)
3	79	F	Meta. Breast (Ad)	Pericardium	36 × 25	CT (calc. -), PET/CT (SUV_{max} 9.0)
4	47	F	Meta. Uterine (LMS)	LA	31 × 17	CT (sessile, calc. -), PET/CT (SUV_{max} 12.6)
5	59	M	Meta. Lung (LMS)	IM (Septum)	16 × 15	CT (calc. -), MRI (iso-intensity on T1WI, hyper-intensity on T2WI, no mobility, CE+)
6	50	F	ML (NHL, CTCL)	RA	46 × 35	CT (calc. -), MRI (iso-intensity on T1WI, hyper-intensity on fat-suppressed T2WI, no mobility, CE+), PET/CT (SUV_{max} 5.6)
Benign lesions						
7	82	M	Myxoma	LA	45 × 35	CT (pedunculated, calc. + +), MRI (iso-intensity on T1WI, hyper-intensity on fat-suppressed T2WI, mobility +)
8	67	F	Myxoma	LA	33 × 23	CT (pedunculated, calc. -), MRI (iso-intensity on T1WI, hyper-intensity on T2WI, mobility +, CE+)
9	85	F	Myxoma	LA	20 × 14	CT (pedunculated, calc. -)
10	85	F	Myxoma	LV	10 × 10	CT (pedunculated, calc. -)
11	71	M	Myxoma	LA	17 × 14	CT (pedunculated, calc. -)
12	64	F	PF	Aortic valve	7 × 5	CT (pedunculated, calc. -)
13	55	M	PF	LA	17 × 13	CT (pedunculated, calc. -)
14	69	M	PF	Aortic valve	5 × 4	CT (pedunculated, calc. -)
15	75	M	PF	Aortic valve	11 × 7	CT (pedunculated, calc. -)
16	75	M	PF	Aortic valve	6 × 5	CT (pedunculated, calc. -)
17	60	F	Vegetation	Mitral valve	-	CT (sessile, calc. ++)
18	80	F	Thrombus	LA	35 × 23	CT (calc. +), PET/CT (no increased uptake)
19	71	M	Thrombus	LV	19 × 12	CT (multi-legged, calc. -)
20	80	F	Thrombus	LA	51 × 37	CT (multi-legged, calc. -)
21	16	F	Lipoma	IM	101 × 86	CT (calc. -)
22	1 m	M	RM	LV	28 × 26	CT (calc. -), MRI (iso-intensity on T1WI, hyper-intensity on T2WI)

No.9 and No.10 lesions were in the same patient. No.12 and No.17 were in the same patient. m: month, F: female, M: male, Meta.: metastasis, Sq: squamous cell carcinoma, Ad: adenocarcinoma, LMS: leiomyosarcoma, ML: malignant lymphoma, NHL: non-Hodgkin's lymphoma, CTCL: cutaneous T cell lymphoma, PF: papillary fibroelastoma, RM: rhabdomyoma, LA: left atrium, LV: left ventricle, RA: right atrium, RV: right ventricle, IM: intramyocardial, calc.: calcification, iso: iso-intensity, hyper: hyper-intensity, CE: contrast enhancement on MRI, SUVmax: maximum standardized uptake value.

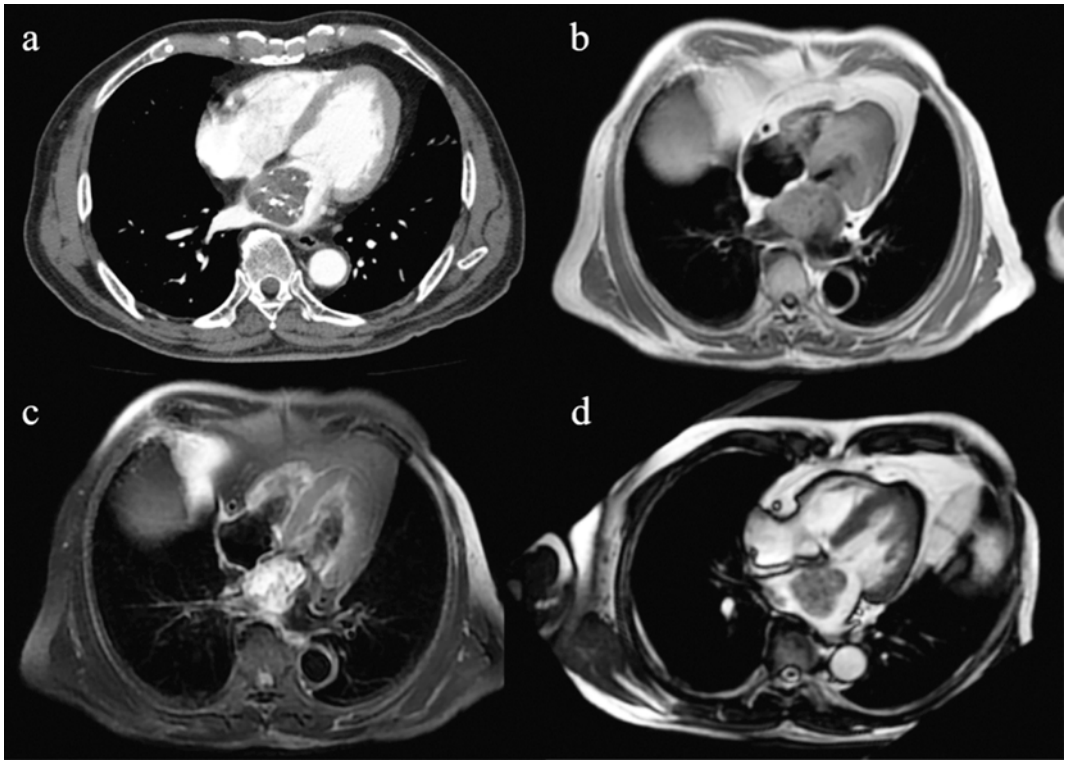

Fig. 3 Cardiac myxoma (Patient No. 7, 82-year-old male). (**a**) Contrast-enhanced CT image, (**b**) T1-weighted black blood image, (**c**) fat-suppressed T2-weighted black blood image, and (**d**) cine image. A mass lesion with a pedunculated base portion was located in the left atrium, and had multiple small calcifications by CT, iso-intensity on T1-weighted imaging, hyper-intensity on fat-suppressed T2-weighted imaging, and mobility by cine imaging.

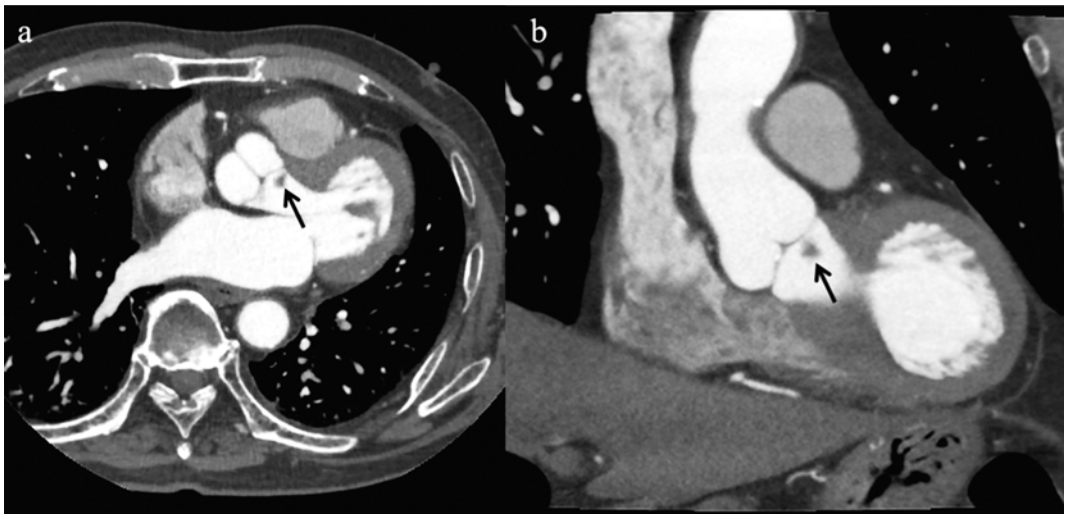

Fig. 4 Papillary fibroelastoma (Patient No. 16, 75-year-old male). ECG-gated contrast-enhanced CT (**a**) axial image and (**b**) coronal image. A low-density mass lesion (size: 6×5 mm) was attached to the aortic valve via a short stalk (arrows).

One thrombus located to the left atrium, and the other was attached to the apex of the LV.

MRI findings

All lesions (3 metastases, 1 malignant lymphoma, and 2 cardiac myxomas) showed iso-intensity on T1WI and showed hyper-intensity on T2WI. All lesions (3 metastases, 1 malignant lymphoma, and 1 cardiac myxoma) showed positive contrast enhancement after the intravenous gadolinium injection. Four malignant tumors (3 metastases and 1 malignant lymphoma) showed no mobility, while 2 cardiac myxomas showed mobility by cine imaging (0/4 (0%) vs. 2/2 (100%) p=0.0667) (Fig. 9).

^{18}F-FDG PET/CT findings

Among the four patients who underwent ^{18}F-FDG PET/CT,

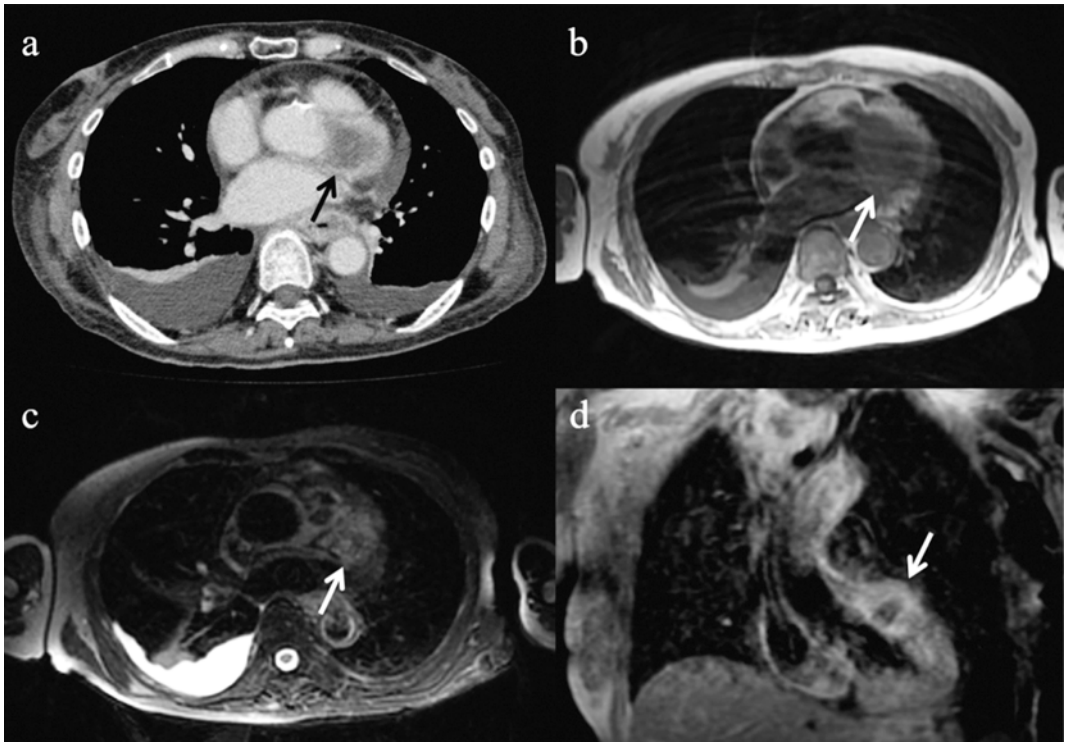

Fig. 5 Metastasis (Patient No. 2, 62-year-old female). (**a**) Contrast-enhanced CT image, (**b**) T1-weighted black blood image, (**c**) fat-suppressed T2-weighted black blood image, and (**d**) gadolinium-enhanced T1-weighted image. A poorly marginated mass lesion in the left ventricle had a sessile base portion with no calcification by CT, and had iso-intensity on T1-weighted imaging, inhomogeneous predominantly high signal intensity on fat-suppressed T2-weighted imaging, and ring-like enhancement by T1-weighted imaging after gadolinium (arrows).

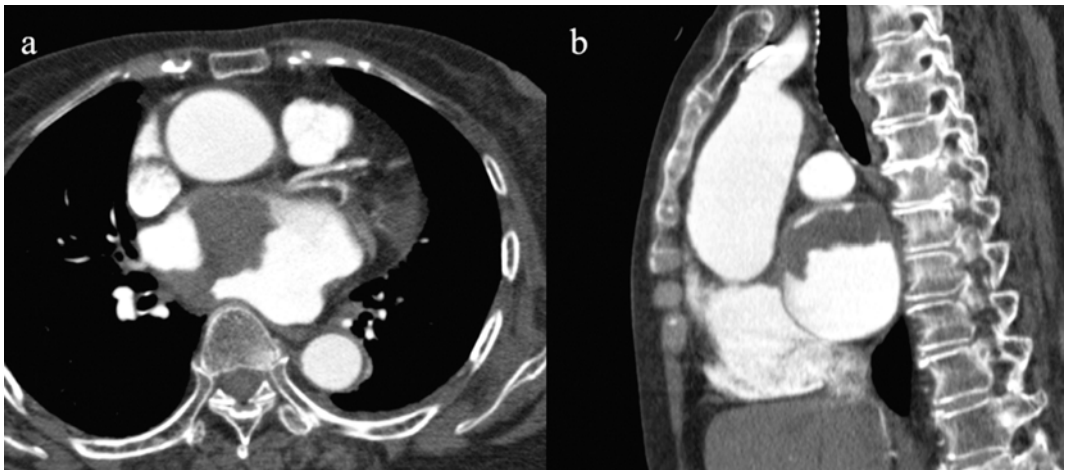

Fig. 6 Thrombus (Patient No. 20, 80-year-old female). Contrast-enhanced gating CT (**a**) axial and (**b**) sagittal image. A low-density mass lesion in the left atrium had no calcification with attachment to the anterior and posterior walls (multi-legged base portion).

three showed LV physiological myocardial ^{18}F-FDG uptake. All cardiac mass lesions located in places other than the LV. Thus, FDG-positive lesions were able to differentiate from LV physiological myocardial uptake. All three malignant lesions (2 metastases and 1 malignant lymphoma) showed visually strong uptake by ^{18}F-FDG PET/CT. The mean SUV_{max} was 9.1 ± 3.5 (5.6 to 12.6). One benign lesion (a thrombus) did not show increased ^{18}F-FDG uptake. In each of these cardiac mass lesions, the morphology of the base portion was observed by enhanced CT and mobility was detected by cine MRI. One cardiac metastasis showed a sessile base portion by enhanced CT and had significantly high ^{18}F-FDG uptake (SUV_{max} 12.6). One mass lesion with malignant lymphoma had no mobility by cine MRI and high ^{18}F-FDG uptake (SUV_{max} 5.6). Details of the findings obtained from whole-body PET/CT images in the 4 patients are as follows: 1. No local recurrence of breast cancer, lymph node metastasis, or distant metastasis was observed in the patient who underwent right mastectomy for

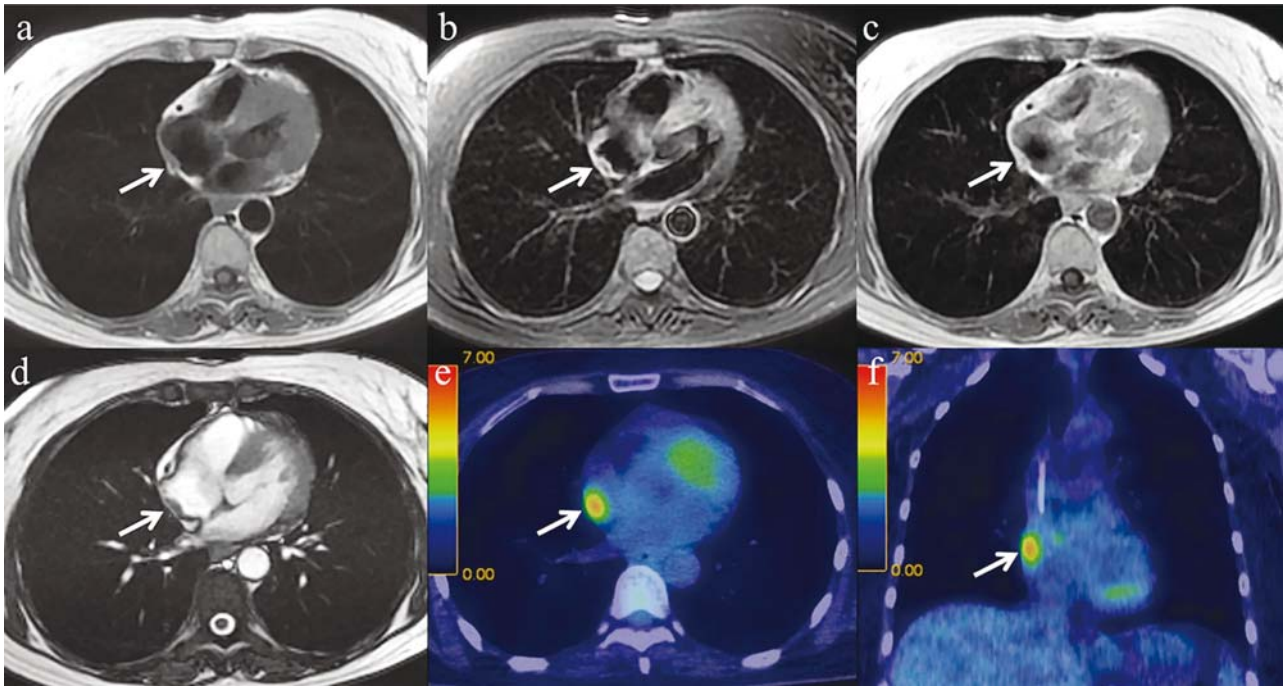

Fig. 7 Non-Hodgkin's malignant lymphoma relapse (Patient No. 6, 50-year-old female). (**a**) T1-weighted black blood image, (**b**) fat-suppressed T2-weighted black blood image, (**c**) gadolinium-enhanced T1-weighted black blood image, (**d**) cine image, and by ^{18}F-FDG PET/CT, (**e**) axial image, and (**f**) coronal image. A nodular lesion was attached to the right atrium free wall (arrows), and had iso-intensity on T1-weighted imaging, hyper-intensity on fat-suppressed T2-weighted imaging, enhancement by T1-weighted imaging after gadolinium, no mobility by cine imaging, and a high FDG uptake by PET/CT (SUV_{max} 5.6).

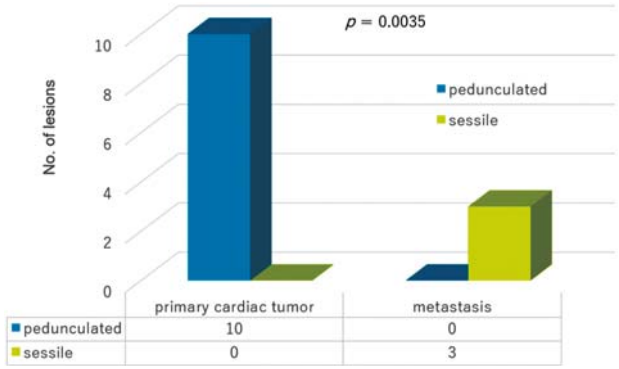

Fig. 8 Comparison of the morphology of the base portion of primary cardiac tumors and metastases. All primary cardiac tumors (5 cardiac myxomas and 5 papillary fibroelastomas) had a pedunculated base portion, and three metastases located in the cavity had a sessile base portion (p=0.0035).

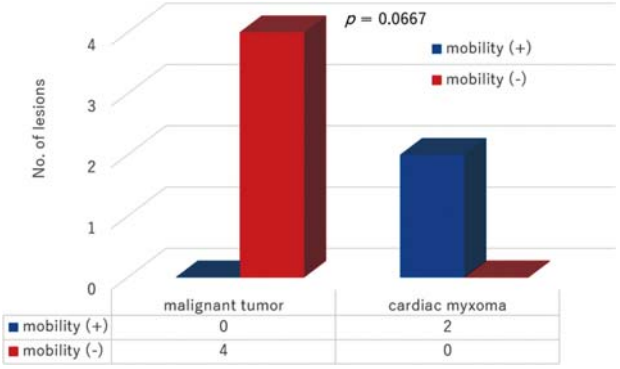

Fig. 9 Comparison of the mobility of malignant tumors and cardiac myxomas on cine MRI. None of the malignant tumors (3 metastases and 1 malignant lymphoma) exhibited mobility, whereas two cardiac myxomas had mobility by cine imaging (p=0.0667).

breast cancer. 2. Cardiac metastasis and muscle metastasis of the left shoulder were observed in the patient with a post-operative state of uterine leiomyoma. 3. A recurrent lesion was confined to the right atrium in the patient with a post-chemotherapy state of non-Hodgkin's malignant lymphoma, and there was no evidence of hepatosplenomegaly or lymph node lesions. 4. A lumbar compression fracture and nasal polyp were observed in the patient with a thrombus in the left atrium.

Discussion

Several types of cardiac mass lesions may be found in specific locations. Detecting the locations of these cardiac masses is a key issue for diagnosis of pathology of the cardiac mass. In the present study, 4 out of 5 (80%) cardiac myxomas located in the left atrium, which is reported to be the most common location of cardiac myxomas (60-75%) (29). In addition, 4 out of 5 (80%) papillary fibroelastomas located in the aortic valve, and 80% of fibroelastomas were found on the

aortic or mitral valves (30). The present results on the locations of cardiac masses are consistent with previous findings (21, 23). In contrast, cardiac metastases located in several different areas (the left ventricle, left atrium, right ventricle, pericardium, and septum) in the present study. The most common site of cardiac involvement of metastases is the pericardium (9). Metastases to the myocardium may occur in any cardiac chamber (22).

The morphology of the base portion may also be useful for diagnosing the type of cardiac mass lesion. All five cardiac myxomas had a pedunculated base portion, as did all five papillary fibroelastomas. Cardiac myxomas and papillary fibroelastomas have a pedunculated base portion, whereas cardiac myxomas typically have a particularly narrow pedicle (20, 23). All three metastases located in the cardiac cavity had a sessile base portion. A significant difference was observed in the morphology of the base portion between primary cardiac tumors (cardiac myxomas and papillary fibroelastomas) and metastases. The difference in the base portion was particularly useful for differentiating between these two groups.

Vegetation also had a sessile base portion. In previous studies, a vegetation length >10 mm, pedunculated, and mobility were predictors for the embolism (31, 32). A differential diagnosis for vegetation generally requires differentiation between a thrombus and fibroelastoma (33). However, as in our study, vegetation had a sessile base portion and the patient had cancer. There are difficulties associated with differentiating between vegetation and metastases because the base portion is similar. The two thrombi showed the characteristic morphology of a multi-legged base portion, which is a finding suggestive of a thrombus. A thrombus is one of the most common cardiac masses and is typically found in the left atrium (19). The attachment portion may be broad-based with little-to-no motion on cine MRI images. However, a thrombus may occasionally be pedunculated, mimicking a myxoma (22). In the present study, a thrombus showed the atypical, but characteristic morphological feature of a multi-legged base portion.

CT is useful for the detection of calcification. Calcification was observed in two benign lesions (1 cardiac myxoma and 1 thrombus). The maximum CT number of the calcified parts in cardiac myxoma was 1111 HU, and that in the thrombus was 154 HU. Previous studies reported calcification in approximately 14% of cardiac myxomas and it was more frequent in right-sided myxomas (29, 34, 35). Few studies have focused on the CT number of calcified parts in cardiac myxomas or thrombi. Therefore, the typical CT range has not yet been clarified. CT and MRI were both performed for one of the two cardiac myxoma lesions. Calcification was easy to detect by CT, but not by MRI. Some benign cardiac lesions (myxomas and fibromas) may contain small foci of calcification (23). Cardiac osteosarcoma has characteristically large foci of calcification (23). Attention is necessary for the differentiation of osteosarcoma because calcification sometimes suggests a benign lesion. Calcification may also be observed in cases of metastasis to the myocardium such as the liver or lung metastasis in colon cancer. It is relatively easy to identify lipoma because of its high fat density (36).

Mobility by cine MRI imaging was useful for differentiating cardiac myxomas from malignant cardiac mass lesions in the current study. All lesions (3 metastases, 1 malignant lymphoma, and 2 cardiac myxomas) with cine MRI data had iso-intensity on T1WI and hyper-intensity on T2WI. All lesions (3 metastases, 1 malignant lymphoma, and 1 cardiac myxoma) with the gadolinium injection had positive contrast enhancement. Difficulties were associated with differentiating between these mass lesions based on the intensity of the cardiac mass lesion and contrast enhancement. However, MRI provides clear information on mass mobility. There was no significant difference in mobility by cine MRI between cardiac myxomas and malignant lesions (metastases and malignant lymphoma). All malignant lesions (3 metastases and 1 malignant lymphoma) had no mobility by cine imaging. In contrast, both benign lesions (2 cardiac myxomas) had mobility. Previous studies reported that the morphological feature of immobility by cardiac MRI and echocardiography was predictive characteristic of malignancy (37). Consistent with these findings, four malignant cardiac mass lesions in the present study had no mobility. Cardiac myxomas may sometimes be attached to the wall, but are often mobile (14), and the two cardiac myxomas in the present study were also typically mobile. Mobility by cine imaging is important for differentiating between benign cardiac mass lesions and malignant cardiac mass lesions.

Malignant and benign lesions may also be differentiated based on the uptake of ^{18}F-FDG by the cardiac mass lesion and visualized by PET/CT. Since the thrombus did not show increased ^{18}F-FDG uptake, we assumed that this cardiac mass was not a malignant lesion. We may more strongly consider a cardiac mass lesion to be malignant if multiple findings, such as a sessile base portion by enhanced CT, high ^{18}F-FDG uptake, and no mobility by cine MRI, suggested malignancy. However, not all cardiac benign mass lesions showed low ^{18}F-FDG uptake. Pseudotumors of the left and right coronary arteries in patients with immunoglobulin G4-related diseases showed increased uptake by ^{18}F-FDG PET/CT (38). Some benign cardiac mass lesions show increased ^{18}F-FDG uptake, whereas primary malignant cardiac tumors and metastatic tumors generally had significantly stronger glucose uptake than primary benign cardiac tumors (27, 28). The optimal SUV_{max} cut-off for differentiating between malignant and benign cardiac lesions was proposed to be 3.5-.0 (27, 28). The

cardiac mass lesions analyzed by ^{18}F-FDG PET/CT in the present study were correctly differentiated by this cut-off value.

Since whole-body images may be easily obtained using ^{18}F-FDG PET/CT, the examinations may reveal that important findings of various sites other than the heart. The acquisition of a whole-body image allows us to confirm that there is no metastatic lesion other than cardiac metastasis or identify completely different diseases such as a compression fracture of the lumbar vertebrae. ^{18}F-FDG PET/CT has the advantage of allowing the whole body to be assessed.

Limitations

The present study has several limitations. This study was performed at a single institution and relatively few cases were evaluated. Furthermore, bias due to inconsistencies in the diagnostic procedures employed through a retrospective study cannot be completely eliminated. This study was a retrospective study that included cardiac masses detected by echocardiography, and metastatic tumors, malignant lymphoma, and lesions different from the original disease found by chance during the whole-body evaluation of these tumors. MRI was performed when internal properties needed to be evaluated, while cine MRI or echocardiography was employed in order to confirm the morphology of the base portion and mobility of cardiac lesions. Since the imaging modality considered to be the most useful for cardiac lesions in each case was performed, the modality was not unified. The imaging modality employed varied among patients, and MRI and ^{18}F-FDG PET/CT were performed on a small number of cases. Another limitation is that ^{18}F-FDG-PET/CT was performed with routine preparation for oncology PET, but without special preparatory steps such as long-term fasting and a low-carbohydrate diet to reduce physiological left ventricle FDG uptake, which is known to affect the evaluation of uptake by cardiac mass lesions. Although all cardiac mass lesions were located in places other than the left ventricle, physiological uptake may mask cardiac and pericardial lesions and make it difficult to differentiate whether focal uptake is abnormal. In addition, CECT was not performed on all lesions. Conventional CECT was performed on most cases, while CT with electrocardiographic gating, which minimizes motion-related artifacts and provides cine-imaging and high-quality images with superior spatial resolution, was employed for a few cases. Moreover, not all cardiac mass lesions were histologically confirmed; however, 7 out of 22 cardiac lesions (5 metastases, 1 malignant lymphoma, and 1 thrombus) were clinically diagnosed.

Conclusions

Two characteristics such as the morphology of the base portion on CT images and mobility by cine MRI are useful for differentiating between malignant and benign cardiac mass lesions. Therefore, cardiac mass lesions may be differentiated based on cardiac imaging. However, cardiac mass lesions vary in certain aspects, and some have characteristic locations, morphologies of the base portion, mobilities, and metabolism of ^{18}F-FDG PET/CT. The morphology of the base portion is useful for differentiating between primary cardiac tumors and metastases. The accurate diagnosis of cardiac mass lesions requires a careful assessment of characteristic findings obtained from imaging modalities.

Acknowledgments

None.

Sources of funding

None.

Conflicts of interest

The authors have no conflict of interest to disclose with respect to this work.

Reprint requests and correspondence:
Hideki Otsuka, MD, PhD
Department of Medical Imaging/Nuclear Medicine, Institute of Biomedical Sciences, Tokushima University Graduate School, 3-18-15 Kuramoto-cho, Tokushima 770-8503, Japan
E-mail: hideki.otsuka@tokushima-u.ac.jp

References

1. Amano J, Nakayama J, Yoshimura Y, et al. Clinical classification of cardiovascular tumors and tumor-like lesions, and its incidences. Gen Thorac Cardiovasc Surg 2013; 61: 435-47.
2. Butany J, Leong SW, Carmichael K, et al. A 30-year analysis of cardiac neoplasms at autopsy. Can J Cardiol 2005; 21: 675-80.
3. Lam KY, Dickens P, Chan AC. Tumors of the heart. A 20-year experience with a review of 12,485 consecutive autopsies. Arch Pathol Lab Med 1993; 117: 1027-31.
4. Takahashi A, Otsuka H, Harada M. Multimodal cardiovascular imaging of cardiac tumors. Ann Nucl Cardiol 2016; 2: 61-7.
5. McAllister H, Fenoglio J. Tumors of the cardiovascular system. In: Hartmann W, Cowan W, eds. Atlas of Tumor Pathology. Washington, DC: Armed Forces Institute of Pathology 1978: 1-20.
6. Butany J, Nair V, Naseemuddin A, et al. Cardiac tumours: diagnosis and management. Lancet Oncol 2005; 6: 219-28.
7. Goldberg AD, Blankstein R, Padera RF. Tumors metastatic to the heart. Circulation 2013; 128: 1790-4.
8. Chiles C, Woodard PK, Gutierrez FR, et al. Metastatic

involvement of the heart and pericardium: CT and MR imaging. Radiographics 2001; 21: 439-49.
9. Klatt EC, Heitz DR. Cardiac metastases. Cancer 1990; 65: 1456-9.
10. Paraskevaidis IA, Michalakeas CA, Papadopoulos CH, et al. Cardiac tumors. ISRN Oncol 2011; 2011: 208929.
11. Kamiya H, Yasuda T, Nagamine H, et al. Surgical treatment of primary cardiac tumors: 28 years' experience in Kanazawa University Hospital. Jpn Circ J 2001; 65: 315-19.
12. Patel R, Lim RP, Saric M, et al. Diagnostic performance of cardiac magnetic resonance imaging and echocardiography in evaluation of cardiac and paracardiac masses. Am J Cardiol 2016; 117: 135-40.
13. Zitzelsberger T, Eigentler TK, Krumm P, et al. Imaging characteristics of cardiac metastases in patients with malignant melanoma. Cancer Imaging 2017; 17: 19.
14. Randhawa K, Ganeshan A, Hoey ET. Magnetic resonance imaging of cardiac tumors: part 1, sequences, protocols, and benign tumors. Curr Probl Diagn Radiol 2011; 40: 158-68.
15. Randhawa K, Ganeshan A, Hoey ET. Magnetic resonance imaging of cardiac tumors: part 2, malignant tumors and tumor-like conditions. Curr Probl Diagn Radiol 2011; 40: 169-79.
16. Gulati G, Sharma S, Kothari SS, et al. Comparison of echo and MRI in the imaging evaluation of intracardiac masses. Cardiovasc Intervent Radiol 2004; 27: 459-69.
17. Choi PW, Kim CN, Chang SH, et al. Cardiac metastasis from colorectal cancer: a case report. World J Gastroenterol 2009; 15: 2675-8.
18. Kim EY, Choe YH, Sung K, et al. Multidetector CT and MR imaging of cardiac tumors. Korean J Radiol 2009; 10: 164-75.
19. Motwani M, Kidambi A, Herzog BA, et al. MR imaging of cardiac tumors and masses: a review of methods and clinical applications. Radiology 2013; 268: 26-43.
20. Guidelines for clinical use of FDG PET, PET/CT 2012. Jpn J Nucl Med (Kaku Igaku). 2012; 49: 391-401.
21. Kassop D, Donovan MS, Cheezum MK, et al. Cardiac masses on cardiac CT: a review. Curr Cardiovasc Imaging Rep 2014; 7: 9281.
22. Rajiah P, Kanne JP, Kalahasti V, et al. Computed tomography of cardiac and pericardiac masses. J Cardiovasc Comput Tomogr 2011; 5: 16-29.
23. Chu LC, Johnson PT, Halushka MK, et al. Multidetector CT of the heart: spectrum of benign and malignant cardiac masses. Emerg Radiol 2012; 19: 415-28.
24. O'Donnell DH, Abbara S, Chaithiraphan V, et al. Cardiac tumors: optimal cardiac MR sequences and spectrum of imaging appearances. AJR Am J Roentgenol 2009; 193: 377-87.
25. Pazos-López P, Pozo E, Siqueira ME, et al. Value of CMR for the differential diagnosis of cardiac masses. JACC Cardiovasc Imaging 2014; 7: 896-905.
26. Kaminaga T, Takeshita T, Kimura I. Role of magnetic resonance imaging for evaluation of tumors in the cardiac region. Eur Radiol 2003; 13: L1-10.
27. Shao D, Wang SX, Liang CH, et al. Differentiation of malignant from benign heart and pericardial lesions using positron emission tomography and computed tomography. J Nucl Cardiol 2011; 18: 668-77.
28. Rahbar K, Seifarth H, Schäfers M, et al. Differentiation of malignant and benign cardiac tumors using 18F-FDG PET/CT. J Nucl Med 2012; 53: 856-63.
29. Grebenc ML, Rosado-de-Christenson ML, Green CE, et al. Cardiac myxoma: imaging features in 83 patients. Radiographics 2002; 22: 673-89.
30. Araoz PA, Mulvagh SL, Tazelaar HD, et al. CT and MR imaging of benign primary cardiac neoplasms with echocardiographic correlation. Radiographics 2000; 20: 1303-19.
31. Okonta KE, Adamu YB. What size of vegetation is an indication for surgery in endocarditis? Interact Cardiovasc Thorac Surg 2012; 15: 1052-6.
32. Hill EE, Herijgers P, Claus P, et al. Clinical and echocardiographic risk factors for embolism and mortality in infective endocarditis. Eur J Clin Microbiol Infect Dis 2008; 27: 1159-64.
33. Grob A, Thuny F, Villacampa C, et al. Cardiac multidetector computed tomography in infective endocarditis: a pictorial essay. Insights Imaging 2014; 5: 559-70.
34. Hoey ET, Mankad K, Puppala S, et al. MRI and CT appearances of cardiac tumours in adults. Clin Radiol 2009; 64: 1214-30.
35. Yılmaz R, Demir AA, Önür İ, et al. Cardiac calcified amorphous tumors: CT and MRI findings. Diagn Interv Radiol 2016; 22: 519-24.
36. Singh S, Singh M, Kovacs D, et al. A rare case of a intracardiac lipoma. Int J Surg Case Rep 2015; 9: 105-8.
37. Patel R, Lim RP, Saric M, et al. Diagnostic performance of cardiac magnetic resonance imaging and echocardiography in evaluation of cardiac and paracardiac masses. Am J Cardiol 2016; 117: 135-40.
38. Kusunose K, Hotchi J, Takagawa Y, et al. Serial imaging changes during treatment of immunoglobulin G4-related disease with multiple pseudotumors. Circulation 2015; 131: 1882-3.